

This is an Open Access document downloaded from ORCA, Cardiff University's institutional repository:<https://orca.cardiff.ac.uk/id/eprint/164887/>

This is the author's version of a work that was submitted to / accepted for publication.

Citation for final published version:

Klaver, Martijn, Yogodzinski, Gene, Albert, Capucine, Camejo-Harry, Michal, Elburg, Marlina, Hoernle, Kaj, Macpherson, Colin, Nowell, Geoff, Rushmer, Tracy, Williams, Helen and Millet, Marc-Alban 2024. Widespread slab melting in modern subduction zones. *Earth and Planetary Science Letters* 626 , 118544. 10.1016/j.epsl.2023.118544

Publishers page: <http://dx.doi.org/10.1016/j.epsl.2023.118544>

Please note:

Changes made as a result of publishing processes such as copy-editing, formatting and page numbers may not be reflected in this version. For the definitive version of this publication, please refer to the published source. You are advised to consult the publisher's version if you wish to cite this paper.

This version is being made available in accordance with publisher policies. See <http://orca.cf.ac.uk/policies.html> for usage policies. Copyright and moral rights for publications made available in ORCA are retained by the copyright holders.



1 Widespread slab melting in modern subduction zones

2 Martijn Klaver^{1*}, Gene Yogodzinski², Capucine Albert¹, Michal Camejo-Harry³, Marlina Elburg⁴, Kaj Hoernle⁵,
3 Colin Macpherson⁶, Geoff Nowell⁶, Tracy Rushmer⁷, Helen Williams^{6,8}, and Marc-Alban Millet¹

4 ¹School of Earth and Environmental Science, Cardiff University, Main Building, Park Place, Cardiff CF10 3AT,
5 United Kingdom

6 ²School of Earth, Ocean, and Environment, University of South Carolina, Columbia, SC 29208-3402, United
7 States

8 ³Department of Earth Sciences, University of Oxford South Parks Road, Oxford OX1 3AN, United Kingdom

9 ⁴Department of Geology, University of Johannesburg, PO Box 524, Auckland Park 2006, South Africa

10 ⁵GEOMAR Helmholtz Centre for Ocean Research Kiel, Wischhofstrasse 1-3, 24148 Kiel, Germany

11 ⁶Department of Earth Sciences, Durham University, South Road, Durham DH1 3LE, United Kingdom

12 ⁷Faculty of Science and Engineering, Macquarie University, 7 Wally's Walk (E6B) Level One, NSW 2109,
13 Australia

14 ⁸Department of Earth Sciences, University of Cambridge, Cambridge CB2 3EQ, United Kingdom

15 *Corresponding author: klaverm@cardiff.ac.uk

17 ABSTRACT

18 It is still a matter of intense debate to what extent partial melting of the subducting slab contributes to arc
19 magmatism in modern subduction zones. In particular, it is difficult to differentiate between silicate melts
20 formed by partial melting of the slab, and aqueous fluids released during subsolidus dehydration as the main
21 medium for slab-to-mantle wedge mass transfer. Here we use $\delta^{49/47}\text{Ti}$ (the deviation in $^{49}\text{Ti}/^{47}\text{Ti}$ of a sample to
22 the OL-Ti reference material) as a robust geochemical tracer of slab melting. Hydrous partial melting of
23 subducted oceanic crust and the superjacent sedimentary layer produces silicic melts in equilibrium with
24 residual rutile. Modelling shows that such silicic slab melts have notably higher $\delta^{49/47}\text{Ti}$ (+0.24±0.06‰) than
25 their protolith due to the strong preference of rutile for the lighter isotopes of Ti. In contrast, even highly
26 saline fluids cannot carry Ti from the slab and hence hydrous peridotite partial melts have $\delta^{49/47}\text{Ti}$ similar to
27 mid-ocean ridge basalts (MORB; ca. 0‰).

28 Primitive (Mg# ≥ 60) arc lavas from eight subduction zones that are unaffected by fractional
29 crystallisation of Fe-Ti oxides show a more than tenfold larger variation in $\delta^{49/47}\text{Ti}$ than found in MORB. In
30 particular, primitive arc lavas display a striking correlation between SiO_2 content and $\delta^{49/47}\text{Ti}$ that ranges
31 from island arc basalts overlapping with MORB, to primitive rhyodacites with $\delta^{49/47}\text{Ti}$ up to 0.26‰
32 erupted in the western Aleutian arc. The elevated $\delta^{49/47}\text{Ti}$ of these primitive arc lavas provides conclusive
33 evidence for partial melts of the slab as a key medium for mass transfer in subduction zones. The Aleutian
34 rhyodacites represent a rare example of slab melts that have traversed the mantle wedge with minimal
35 modification. More commonly, slab melts interact with the mantle wedge to form an array of primary arc
36 magmas that are a blend of slab- and peridotite-derived melt. We identify primitive arc lavas with a
37 clearly resolvable slab melt signature in all eight subduction zone localities, confirming that slab melting is
38 prevalent in modern subduction zones.

39
40 **Keywords:** Slab melting; Titanium isotopes; Rutile; Subduction zone; Aleutian arc

41 42 **Highlights**

- 43 • Global primitive arc lavas (Mg# ≥ 60) display notable $\delta^{49/47}\text{Ti}$ heterogeneity
- 44 • Residual rutile imposes high $\delta^{49/47}\text{Ti}$ of $0.24 \pm 0.06\text{‰}$ on hydrous, silicic slab melts
- 45 • Primitive Aleutian rhyodacites have the same $\delta^{49/47}\text{Ti}$ as predicted for slab melts
- 46 • A variably diluted signature of slab melts is found in all eight subduction zones
- 47 • A slab melt component is required to generate silicic primitive arc lavas

48 49 **1. Introduction**

50 Subduction zones are a nexus of geochemical cycles and link the crust, hydrosphere, atmosphere, and Earth's
51 mantle. Mass transfer from subducting slabs is a likely trigger for partial melting of the overlying mantle
52 wedge, giving rise to arc lavas with a ubiquitous geochemical signature of subducted oceanic crust and its
53 sedimentary cover (e.g., Gill, 1981; Tera et al., 1986; White and Dupré, 1986; Plank and Langmuir, 1993; Elliott
54 et al., 1997). Despite the key role in modulating the composition of the continental crust, deep mantle, and
55 Earth's surface habitat, the mechanisms of mass transfer in subduction zones are still not well understood

56 (Spandler and Pirard, 2013; Keppler, 2017; Nielsen and Marschall, 2017; Hernández-Urbe et al., 2020; Klaver
57 et al., 2020). A persistent question is to what extent the top of the subducting slab melts in modern subduction
58 zones. Melts are an efficient medium to mobilise trace elements and volatiles from the slab (e.g., Johnson and
59 Plank, 1999; Hermann et al., 2006), and the latest generation of slab thermal models (Syracuse et al., 2010;
60 van Keken et al., 2011; van Keken et al., 2018) and geochemical slab-top thermometers (Cooper et al., 2012)
61 suggest that the hydrous solidus of sediments and altered oceanic crust can be reached in most modern
62 subduction zones. Conversely, saline aqueous fluids might also be capable of carrying a significant budget of
63 trace elements to the mantle wedge source of arc magmas without the need to invoke slab melting (Tatsumi,
64 1989; Keppler, 2017; Rustioni et al., 2021).

65 The trace element and radiogenic isotopic signature of primitive arc lavas unquestionably supports slab-
66 to-mantle wedge mass transfer, but does not provide a conclusive discrimination between slab melting and
67 transport by saline fluids (cf., Rustioni et al., 2021; Li et al., 2022; Turner and Langmuir, 2022b). For instance,
68 either model explains the characteristic relative depletion in Ti, Nb, and Ta displayed by primitive arc lavas. In
69 the sediment melting scenario, this depletion is imposed by the accessory mineral rutile (TiO₂) present in the
70 residue during hydrous melting of eclogite-facies slab lithologies (e.g., Ryerson and Watson, 1987; Yogodzinski
71 et al., 1995; Elliott et al., 1997), whereas in the saline fluid model the relative depletion in Ti, Nb, and Ta results
72 from the negligible solubility of these elements in fluids. Here, we demonstrate that the isotopic composition
73 of Ti in primitive arc lavas is a uniquely diagnostic tracer of the presence of a slab melt component in primitive
74 arc magmas. This approach hinges on the distinct bonding environment of Ti in Fe-Ti oxides. Rutile has a strong
75 preference for the lighter isotopes of Ti compared to silicate minerals and melts (Aarons et al., 2021; Hoare et
76 al., 2022; Rzehak et al., 2022). As a result, partial melts in equilibrium with residual rutile will display the
77 characteristic relative depletion in Ti, Nb, and Ta, as well as distinctly heavier Ti isotope compositions than
78 their protolith. In contrast, experimental studies indicate that aqueous fluids cannot mobilise Ti even at high
79 salinities (e.g., Kessel et al., 2005a; Keppler, 2017; Rustioni et al., 2021), and as rutile is not a stable residual
80 phase during hydrous peridotite melting (Grove et al., 2006; Till et al., 2012), mass transfer by saline fluids
81 alone does not have the capability to impose a distinct Ti isotope signature on primitive arc lavas.

82 We test this hypothesis by combining quantitative Ti isotope fractionation modelling of slab melting with
83 high-precision Ti isotope composition measurements of a comprehensive suite of global primitive arc lavas.

84 This shows that slab melting occurs in all eight subduction zones for which Ti isotope data are available,
85 irrespective of slab age and temperature, and therefore is a widespread feature of modern subduction

86

87 **2. Samples and analytical techniques**

88 We present new Ti isotope composition data for 52 extrusive volcanic samples from six subduction zone
89 localities. These comprise the Aegean arc (Nisyros and Santorini), Aleutian arc (Adak and dredge samples from
90 the Komandorsky Straits and Western Cones area), Lesser Antilles arc (Bequia, Grenada, Saba, and St. Vincent),
91 Philippines arc (Surigao Peninsula, Mindanao), Solander Islands (New Zealand), and Cook Island (Austral
92 Volcanic Zone, Chile). A detailed description of these localities and the samples is provided in the
93 supplementary material. The new data greatly expand on previously published data (26 samples) for arc lavas
94 from the New Britain arc (Millet and Dauphas, 2014), Mariana arc (Millet et al., 2016), Kermadec arc
95 (Monowai; Hoare et al., 2020), and Aegean arc (Santorini, Kos; Hoare et al., 2020; Greber et al., 2021). Taken
96 together, these localities cover a wide range of subduction zone parameters such as the age of subducted
97 crust (10 to ca. 200 Ma), slab dip (30–70°), and subduction angle (straight versus oblique; see supplementary
98 Table S4). All samples have a minimum of major- and trace element characterisation, in most cases
99 complemented with radiogenic isotope data (compiled in supplementary Dataset 2).

100 For the selection of the new samples, emphasis was placed on primitive lavas that are least affected
101 by magmatic differentiation. We use Mg# (molar $100 \times \text{Mg}/[\text{Mg}+\text{Fe}]$) as discriminant and designate
102 samples with Mg# ≥ 60 as primitive, and samples with Mg# < 60 as evolved. In addition, we specifically
103 targeted primitive arc lavas with a geochemical signature often ascribed to slab melts, such as elevated
104 Sr/Y, fractionated rare earth element patterns, and high SiO₂ content (e.g., Defant and Drummond, 1990).
105 Although such primitive andesites, dacites, and rhyodacites are a volumetrically minor fraction of global
106 arc magmas (Kelemen et al., 2014), they are well-suited to test the sensitivity of Ti isotopes to slab
107 melting. In particular, we include seafloor rhyodacites with high Mg# (64–73) erupted on thin oceanic
108 crust in the western Aleutian arc, which are proposed to be nearly unmodified melts of the subducting
109 Pacific oceanic crust (Yogodzinski et al., 2015; Yogodzinski et al., 2017).

110 Titanium isotope composition measurements were carried out following a well-established protocol
111 described in detail elsewhere (e.g., Millet and Dauphas, 2014; Hoare et al., 2020; Klaver et al., 2021).
112 Briefly, aliquots of dissolved sample corresponding to ca. 5 μg Ti were equilibrated with a ^{47}Ti – ^{49}Ti double

113 spike prior to Ti purification with Eichrom DGA resin. Measurements were performed using a ThermoScientific
114 Neptune Plus (at Durham University) and Nu Plasma II (at Cardiff University) multi-collector inductively-
115 coupled plasma mass spectrometer (MC-ICP-MS) operated in medium resolution mode. Titanium isotope
116 composition data are reported in the conventional delta-notation relative the Origins Laboratory Ti reference
117 material (OL-Ti) as $\delta^{49/47}\text{Ti}_{\text{OL-Ti}}$ (hereafter abbreviated to $\delta^{49/47}\text{Ti}$). Repeat measurements of geological and Ti
118 solution reference materials indicates an intermediate precision of 0.020‰ (2s) for the individual
119 measurements made in Durham (Millet et al., 2016) and 0.030‰ (2s) for those made in Cardiff (supplementary
120 Figure S3). For most samples measured in Cardiff, 2–4 repeat measurements were made (see supplementary
121 Dataset 2). See the supplementary material for more discussion of measurement uncertainties.

122

123 3. Results

124 The primitive arc lavas (whole rock Mg# ≥ 60) in this study vary in major element composition from (picritic)
125 basalts with 46 wt.% SiO₂ and up to 15.5 wt.% MgO (e.g., St. Vincent, Lesser Antilles arc) to high-Mg#
126 rhyodacites (70 wt.% SiO₂, 2.1 wt.% MgO) erupted as submarine lavas on oceanic crust in the western Aleutian
127 arc. Despite the large range in silica content, their high Mg# indicates that these arc lavas are primitive melts
128 that are in or very close to equilibrium with mantle olivine and/or orthopyroxene. As shown in Figure 1,
129 primitive arc lavas display notably heterogeneous $\delta^{49/47}\text{Ti}$ (ca. 0.3‰ variation) compared to normal mid ocean
130 ridge basalts (N-MORB), which have homogeneous $\delta^{49/47}\text{Ti}$ of 0.001 ± 0.015 ‰ (Millet et al., 2016; Deng et al.,
131 2018). Basaltic primitive arc lavas overlap in $\delta^{49/47}\text{Ti}$ with N-MORB but more silica-rich varieties have
132 progressively higher $\delta^{49/47}\text{Ti}$. The high-Mg# rhyodacites from the Aleutian arc have the most extreme $\delta^{49/47}\text{Ti}$ at
133 0.21–0.26‰, but also high-Mg# andesites from the Aegean arc, Philippines arc, Solander Islands, and Cook
134 Island have $\delta^{49/47}\text{Ti}$ clearly elevated relative to N-MORB.

135

136 4. Modelling Ti isotope fractionation during slab melting

137 The contrasting bonding environment of Ti in Fe-Ti oxides compared to silicate minerals and melts is the
138 fundamental parameter that introduces Ti isotope heterogeneity during magmatic processes (e.g., Millet et al.,
139 2016; Deng et al., 2019; Hoare et al., 2020). Titanium isotope fractionation between silicate minerals (e.g.,
140 pyroxene, garnet) and silicate melt is negligible and, as a result, partial melting of peridotite produces melts
141 with essentially the same $\delta^{49/47}\text{Ti}$ as their protolith (Figure 2; Hoare et al., 2022). Conversely, Fe-Ti oxide

142 minerals, notably rutile, have a strong preference for the lighter isotopes of Ti relative to silicates (Aarons et
1 al., 2021; Hoare et al., 2022; Rzehak et al., 2022). As a result, the presence of rutile in the residue during partial
2 143 melting will aid the retention of Ti and impose an isotopically heavy Ti isotope signature on the partial melt.
3
4 144

5
6 145 Rutile is a stable residual phase during hydrous partial melting of eclogite-facies metabasite and
7
8 146 metasediment due to the low solubility of TiO₂ in the silicic partial melts produced at 750–1000 °C
9
10 147 (Ryerson and Watson, 1987; Gaetani et al., 2008; Xiong et al., 2009). We use experimentally determined
11
12 148 melting reactions of such slab lithologies coupled with mineral–melt Ti isotope fractionation factors to
13
14 149 model the magnitude of Ti isotope fractionation that occurs during melting in the presence of residual
15
16 150 rutile. Rutile is the main repository of Ti in the melting residua of metabasite and metasediment, and the
17
18 151 rutile–melt Ti isotope fractionation factor therefore exerts the dominant control on the magnitude of Ti
19
20 152 isotope fractionation during melting. We employ an average rutile–melt Ti isotope fractionation factor of
21
22 153 $10^3 \ln \alpha_{rt-melt} = -0.444 \pm 0.028 \times 10^6 / T^2$ compiled from two recent studies (Hoare et al., 2022; Rzehak et al.,
23
24 154 2022). The difference in Ti isotope composition between the partial melt and the protolith ($\Delta^{49/47}\text{Ti}_{melt-}$
25
26 155 $protolith$) can then be calculated through isotopic mass balance as described in detail in the supplementary
27
28 156 material. Subsequently, the absolute $\delta^{49/47}\text{Ti}$ of slab melts can be derived by adding $\Delta^{49/47}\text{Ti}_{melt-protolith}$ as
29
30 157 shown in Figure 2 to the $\delta^{49/47}\text{Ti}$ of the protolith ($\delta^{49/47}\text{Ti}_{slab\ melt} = \Delta^{49/47}\text{Ti}_{melt-protolith} + \delta^{49/47}\text{Ti}_{protolith}$).
31
32 158

33
34 159 The water-saturated solidus of eclogite with a composition akin to pristine to altered MORB (0–1.0
35
36 160 wt.% K₂O, 1.2–2.0 wt.% TiO₂) at sub-arc depths (2.6–4.5 GPa) lies between 750 and 800 °C (Schmidt et al.,
37
38 161 2004; Kessel et al., 2005b; Carter et al., 2015; Martin and Hermann, 2018; Sisson and Kelemen, 2018).
39
40 162 These studies find rutile as a residual phase up to at least 900 °C or 25% melting. As a result of the
41
42 163 residual rutile, hydrous, silicic metabasite partial melts (73–79 wt.% SiO₂ on an anhydrous basis) have
43
44 164 notably higher $\delta^{49/47}\text{Ti}$ than their protolith, in clear contrast with the negligible Ti isotope fractionation
45
46 165 during partial melting of rutile-free peridotite (Figure 2a). Metabasite melts formed at 750–800 °C show
47
48 166 the largest Ti isotope fractionation ($\Delta^{49/47}\text{Ti}_{melt-protolith} = 0.21\text{--}0.29\text{‰}$; Figure 2a). At higher temperature,
49
50 167 the diminishing proportion of rutile in the residue leads to progressively lower $\Delta^{49/47}\text{Ti}_{melt-protolith}$. The
51
52 168 MORB protolith of the metabasite has $\delta^{49/47}\text{Ti}$ around zero (Figure 1; Millet et al., 2016; Deng et al., 2018);
53
54 169 hence the absolute $\delta^{49/47}\text{Ti}$ of metabasite partial melts at 750–800 °C is $0.24 \pm 0.06\text{‰}$.
55
56 170

57
58 171 Low-degree hydrous partial melts of eclogite-facies metasediments at 750–950 °C and 3–6 GPa are
59
60 172 also in equilibrium with residual rutile (Skora and Blundy, 2010; Martindale et al., 2013; Mann and
61
62
63
64
65

171 Schmidt, 2015; Skora et al., 2015) and therefore have higher $\delta^{49/47}\text{Ti}$ than their protolith (Figure 2b), unlike
172 what was assumed by Kommescher et al. (2023). Given the lower TiO_2 content of the sedimentary protoliths,
173 the proportion of rutile in the residue is generally smaller and the Ti isotope fractionation effect is more
174 subdued compared to metabasite melting. In several cases, however, titanomagnetite joins rutile as a residual
175 phase. Titanomagnetite has an even stronger preference for the lighter isotopes of Ti than rutile (Hoare et al.,
176 2022) and hence its presence leads to higher $\Delta^{49/47}\text{Ti}_{\text{melt-protolith}}$ (0.3–0.4‰; Figure 2b). As a result,
177 metasediment partial melts have highly variable $\Delta^{49/47}\text{Ti}_{\text{melt-protolith}}$, but are always positively fractionated
178 relative to their protolith. Modern terrigenous sediments have $\delta^{49/47}\text{Ti}$ in the range of 0.16–0.24‰ (Greber et
179 al., 2017; Klaver et al., 2021), meaning that hydrous metasediment partial melts have $\delta^{49/47}\text{Ti}$ ranging from
180 0.25‰ up to 0.6‰.

181

182 5. Discussion

183 5.1. Negligible influence of magmatic differentiation on $\delta^{49/47}\text{Ti}$ of primitive arc lavas

184 Differentiation of arc magmas in the crust modifies their composition and can obscure a mantle source
185 signature. In case of Ti, magma mixing and fractional crystallization cause large $\delta^{49/47}\text{Ti}$ variation in evolved arc
186 lavas (Millet et al., 2016; Hoare et al., 2020; Greber et al., 2021). Several lines of evidence confirm, however,
187 that the variations recorded in our primitive arc lavas represent a primary feature of their source rather result
188 from magmatic differentiation. The removal of isotopically light Fe-Ti oxides, mainly titanomagnetite, during
189 fractional crystallization drives arc magmas to higher $\delta^{49/47}\text{Ti}$ (Deng et al., 2019; Hoare et al., 2020; Hoare et al.,
190 2022) and evolved, low-Mg# rhyodacites from the Aegean arc display $\delta^{49/47}\text{Ti}$ up to 0.7‰ (Figure 3a). Hoare et
191 al. (2020) found that the saturation point of titanomagnetite may be dependent on the water content of arc
192 magmas but generally occurs around Mg# 30–40. The onset of titanomagnetite fractionation causes a notable
193 inflection in both TiO_2 content and $\delta^{49/47}\text{Ti}$ versus Mg# (Figure 3a; Hoare et al., 2022). At higher Mg#, Ti is
194 incompatible with only a small fraction hosted in clinopyroxene during fractional crystallization, which does
195 not cause significant Ti isotope fractionation (Figure 3a). As a result, $\delta^{49/47}\text{Ti}$ of primitive arc lavas (Mg# ≥ 60) is
196 not affected by low-pressure fractional crystallization of Fe-Ti oxides.

197 Crystallisation of garnet at the base of thick crust or in the upper mantle is another mechanism that can
198 generate silicic magmas with a geochemical signature similar to slab melts (e.g., high Sr/Y; Defant and
199 Drummond, 1990), as proposed for instance by Macpherson et al. (2006). High-pressure fractional

200 crystallisation, however, cannot explain the high $\delta^{49/47}\text{Ti}$ as garnet, like other silicate minerals (see
201 supplementary Figure S1), does not fractionate Ti isotopes relative to the melt. Furthermore,
202 studies indicate that, just as found for low-pressure fractional crystallisation (Figure 3a), Fe-Ti oxides are
203 absent in early stages of high-pressure crystallisation (Alonso-Perez et al., 2009; Coldwell et al., 2011) and
204 thus cannot drive an increase in $\delta^{49/47}\text{Ti}$ at $\text{Mg\#} \geq 60$.

205 The high Mg# of primitive arc lavas also precludes significant modification by mixing with evolved
206 magmas with low Mg# and elevated $\delta^{49/47}\text{Ti}$ (Figure 3b). Binary mixing between a basaltic components
207 with $\delta^{49/47}\text{Ti}$ of ca. 0‰ and an evolved Aegean arc andesite (61 wt.% SiO_2 , $\delta^{49/47}\text{Ti} = 0.19\text{‰}$), dacite (65
208 wt.% SiO_2 , $\delta^{49/47}\text{Ti} = 0.43\text{‰}$), or rhyodacite (70 wt.% SiO_2 , $\delta^{49/47}\text{Ti} = 0.69\text{‰}$) forms a much steeper array in
209 $\delta^{49/47}\text{Ti}$ versus SiO_2 space than the primitive arc lavas (Figure 3b). Furthermore, andesites and dacites
210 from Kos (Aegean arc) that formed through extensive hybridization of mafic and felsic melts may have
211 similar $\delta^{49/47}\text{Ti}$ to the primitive arc lavas, but they also have $\text{Mg\#} < 60$ (Greber et al., 2021). In general,
212 there does not exist a mixing solution that can reproduce the combined SiO_2 - $\delta^{49/47}\text{Ti}$ signature of the
213 primitive arc lavas at $\text{Mg\#} \geq 60$.

214 The primitive rhyodacites from western Aleutian arc with $\delta^{49/47}\text{Ti}$ of 0.21–0.26‰ are the most
215 extreme arc lavas in this study and therefore deserve special consideration. The absence of Fe-Ti oxide
216 phenocrysts suggests that these magmas are undersaturated with respect to Fe-Ti oxides. In general, the
217 geochemical variability of lavas from the western Aleutian arc is inconsistent with any plausible fractional
218 crystallisation process, and the complete absence of evolved ($\text{Mg\#} < 55$) samples further attests to the
219 negligible role that intracrustal differentiation plays in this locality (Yogodzinski et al., 2015). Extensive
220 fractional crystallisation of hydrous basaltic magmas in the mantle wedge, including removal of a Fe-Ti
221 oxide phase and concomitant Ti isotope fractionation, followed by re-equilibration with mantle wedge
222 peridotite to re-establish $\text{Mg\#} \geq 60$ (Macpherson et al., 2006) is therefore also unlikely. Furthermore, in
223 such a scenario it would be expected that a broad spectrum of primitive lavas ranging from basalts to
224 rhyodacites are erupted, but only primitive rhyodacites are recovered from the Western Cones area and
225 there is no trace of lavas with lower Mg# or SiO_2 (Yogodzinski et al., 2015). Hence, the unusual Ti isotope
226 variation observed in the western Aleutian rhyodacites and other primitive arc lavas in this study does
227 not result from crustal processes but reflects a primary signature that informs on the mode of slab-to-
228 mantle wedge mass transfer in subduction zones.

229

1
2 **230 5.2. Bulk addition of sediments**
3

4 231 Recycled sediments form a key component of arc magmas and could contribute to the elevated $\delta^{49/47}\text{Ti}$ of
5
6 232 primitive arc lavas. Phanerozoic marine sediments have higher $\delta^{49/47}\text{Ti}$ (0.16–0.24‰; Greber et al., 2017;
7
8 233 Klaver et al., 2021) than N-MORB, but only barely reach the $\delta^{49/47}\text{Ti}$ of primitive rhyodacites from the Aleutian
9
10 234 arc (Figure 4). We investigate the role of sediments by combining $\delta^{49/47}\text{Ti}$ with radiogenic Nd isotopes
11
12 235 ($^{143}\text{Nd}/^{144}\text{Nd}$) that act as a sensitive proxy for recycled sediment. For the Aegean arc there are direct
13
14 236 constraints on $\delta^{49/47}\text{Ti}$ of subducting sediments, which are homogeneous at $0.172\pm 0.012\text{‰}$ and have
15
16 237 $^{143}\text{Nd}/^{144}\text{Nd}$ of 0.5125 (Klaver et al., 2021). Bulk mixing of depleted mantle wedge peridotite with Aegean
17
18 238 sediment causes a rapid decrease in $^{143}\text{Nd}/^{144}\text{Nd}$ but only a subdued increase in $\delta^{49/47}\text{Ti}$ in the peridotite (Figure
19
20 239 4a). Mixing with sediment that has lower $^{143}\text{Nd}/^{144}\text{Nd}$, such as the global subducting sediment average (GLOSS;
21
22 240 Plank and Langmuir, 1998), has an even smaller influence on $\delta^{49/47}\text{Ti}$. Hence, bulk mixing with subducting
23
24 241 sediment can only cause a resolvable Ti isotope effect in primitive arc lavas with highly unradiogenic Nd
25
26 242 isotope compositions. Moreover, partial melting of physical mixtures of sediment and mantle wedge
27
28 243 peridotite, as proposed in the *mélange* model (e.g., Nielsen and Marschall, 2017), does not leave residual rutile
29
30 244 or another Fe-Ti oxide phase (Codillo et al., 2018), and is hence not accompanied by Ti isotope fractionation.
31
32 245 Two samples from the Lesser Antilles arc and one from the Aegean arc with $^{143}\text{Nd}/^{144}\text{Nd} < 0.5129$ show
33
34 246 combined Ti–Nd isotope compositions that can be consistent with bulk sediment mixing. A group of samples
35
36 247 (predominantly from the Lesser Antilles) have $\delta^{49/47}\text{Ti}$ and $^{143}\text{Nd}/^{144}\text{Nd}$ similar to MORB, but the majority of the
37
38 248 primitive arc lavas have rather radiogenic Nd isotope compositions ($^{143}\text{Nd}/^{144}\text{Nd} > 0.5129$) coupled with much
39
40 249 higher $\delta^{49/47}\text{Ti}$ than sediment–peridotite mixtures, indicating that bulk sediment addition cannot account for
41
42 250 the observed Ti isotope heterogeneity of primitive arc lavas.
43
44
45
46
47
48

251

49 **252 5.3. Partial melts in equilibrium with rutile**
50

51 253 The only viable agent that can impose elevated $\delta^{49/47}\text{Ti}$ on primitive arc lavas is a partial melt generated in the
52
53 254 presence of residual rutile. The stability of rutile in a melting residue is an interplay between the Ti content of
54
55 255 the protolith and the solubility of TiO_2 in the partial melt. Rutile solubility increases with temperature and is
56
57 256 much higher in mafic melts than in silicic, alkali-rich melts (Ryerson and Watson, 1987; Gaetani et al., 2008;
58
59 257 Xiong et al., 2009). As such, rutile is not a residual phase during melting of sediment–peridotite mixtures
60
61
62
63
64
65

258 (mélanges) as the TiO₂ solubility in such high-temperature (>1200 °C) mafic partial melts exceeds the TiO₂
259 content of the mélange protolith (Codillo et al., 2018). Furthermore, experimental studies indicate that Ti is
260 highly insoluble in aqueous fluids; even highly saline fluids cannot liberate Ti from the slab (Rustioni et al.,
261 2021) and hence do not have the capability to drastically alter the $\delta^{49/47}\text{Ti}$ of the mantle wedge. When an influx
262 of aqueous fluids causes hydrous melting of mantle wedge peridotite, the Ti content of the peridotite protolith
263 is too low to retain rutile in the residue (e.g., Grove et al., 2006; Till et al., 2012; Pirard and Hermann, 2015). As
264 a result, $\delta^{49/47}\text{Ti}$ of hydrous partial melting of mantle wedge peridotite does not cause Ti isotope fractionation
265 and the resultant melts are therefore expected to have the same $\delta^{49/47}\text{Ti}$ as N-MORB (Figure 5).

266 The oceanic crust and its sedimentary cover provide the only suitable protolith for partial melts in
267 equilibrium with rutile. The Ti content of the protolith is sufficiently high (typically 1–2 wt.% TiO₂ in MORB
268 and 0.5–1 wt.% TiO₂ in sediments), and hydrous partial melting at low temperature produces silicic partial
269 melts in which the solubility of TiO₂ is low but still at least an order of magnitude higher than in fluids.
270 Hence, rutile is retained in the residue up to at least 900 °C and our modelling (see section 4 and Figure 2)
271 shows that partial melts of (altered) oceanic crust formed at 750–800 °C have fractionated $\delta^{49/47}\text{Ti}$
272 (0.24±0.06‰). Partial melts of the subducting slab are therefore the only plausible medium to impart the
273 diagnostic $\delta^{49/47}\text{Ti}$ signature on arc magmas.

274 Moreover, slab melts in equilibrium with residual rutile can adequately explain the characteristic
275 relative depletion in Nb and Ta of global arc magmas (e.g., Ryerson and Watson, 1987; Yogodzinski et al.,
276 1995; Elliott et al., 1997; Turner and Langmuir, 2022a). Negative Nb anomalies by themselves, however,
277 do not provide unambiguous evidence for slab melting. Slab-to-mantle wedge mass transfer by aqueous
278 fluids can also impose a negative Nb anomaly on arc magmas due to the low solubility of Nb and Ta in
279 fluids compared to other incompatible elements (Rustioni et al., 2021), but cannot impose elevated
280 $\delta^{49/47}\text{Ti}$ on primitive arc lavas due to the lack of Ti mobility in such fluids. The difference between fluid-
281 and partial melt-dominated mass transfer is clearly demonstrated by the samples in this study. All
282 primitive arc lavas display clear relative depletions in Nb, but in several basaltic samples with $\delta^{49/47}\text{Ti}$
283 similar to N-MORB, including the majority of the Lesser Antilles samples (Figure 4), negative Nb anomalies
284 are not associated with a fractionated Ti isotope signature (supplementary Figure S6). The lack of
285 elevated $\delta^{49/47}\text{Ti}$ suggests fluid-dominated mass transfer in these Lesser Antilles samples, whereas the

286 combination of relative Nb–Ta depletion and elevated $\delta^{49/47}\text{Ti}$ as seen in other primitive arc lavas in this study
1
2 287 is uniquely attributable to slab melting.
3

4 288 Metabasite partial melts will have the same $^{143}\text{Nd}/^{144}\text{Nd}$ as their protolith (MORB; Figure 4b). Primitive
5
6 289 Aleutian rhyodacites overlap with metabasite partial melts in Ti–Nd isotope space, in agreement with other
7
8 290 geochemical data that suggest a strong slab melt signature in these samples (e.g., Yogodzinski et al., 1995;
9
10 291 Yogodzinski et al., 2015; Yogodzinski et al., 2017). Samples from the other localities have lower $\delta^{49/47}\text{Ti}$, which
11
12 292 suggests that they are not pure slab melts, but these lavas do require a variable contribution of a slab melt to
13
14 293 explain their fractionated Ti isotope compositions. In general, Nd isotopes indicate that the slab melt
15
16 294 component recorded in the primitive arc lavas is predominantly derived from the (altered) oceanic crust with a
17
18 295 subordinate contribution from the superjacent sedimentary veneer. Aegean arc lavas show the strongest
19
20 296 metasediment melt signature, consistent with the thick subducted sediment package that is clearly expressed
21
22 297 in the radiogenic isotope composition of Aegean arc lavas (e.g., Elburg et al., 2014; Klaver et al., 2016).
23
24
25

26 298

27 299 **5.4. How slab melts contribute to arc magmatism**

28
29 300 Hydrous, silicic slab melts are in chemical disequilibrium with mantle wedge peridotite and will react to form
30
31 301 orthopyroxene once released from the slab (e.g., Rapp et al., 1999; Pirard and Hermann, 2015). This reaction
32
33 302 consumes some SiO_2 from the slab melt and leads to an increase in Mg# and compatible element contents (Cr,
34
35 303 Ni) in the reacted melt while incompatible trace element patterns are preserved (e.g., Pirard and Hermann,
36
37 304 2015; Sisson and Kelemen, 2018; Lara and Dasgupta, 2020). Once formed, such orthopyroxene veins can act as
38
39 305 pathways for subsequent batches of slab melt, leading to equilibration of melt Mg# with wall-rock
40
41 306 orthopyroxene but otherwise leaving the major- and trace element signature of the slab melt unaffected
42
43 307 (Rebaza et al., 2023).
44
45

46
47 308 The reaction that forms orthopyroxene veins will have little effect on the $\delta^{49/47}\text{Ti}$ of the percolating slab
48
49 309 melt. Titanium is incompatible in orthopyroxene and hence the extraction of orthopyroxene from the melt will
50
51 310 increase melt Ti content (Sisson and Kelemen, 2018). Equilibrium Ti isotope fractionation between silicate melt
52
53 311 and orthopyroxene is negligible (Rzehak et al., 2021; see supplementary Figure S1). Hence, newly formed
54
55 312 orthopyroxene is predicted to have a Ti isotope composition that mirrors that of the melt and does drive the
56
57 313 melt to notably higher or lower $\delta^{49/47}\text{Ti}$. Even after substantive orthopyroxene formation $\delta^{49/47}\text{Ti}$ of the slab
58
59 314 melt will be thus conserved.
60
61
62
63
64
65

1
2 315 The primitive rhyodacites from the Aleutian arc with $\delta^{49/47}\text{Ti}$ of $0.24\pm 0.03\%$ (Figures 4 and 5) are a
3
4 316 rare example of such a process where silicic slab melts have traversed the mantle wedge with little
5
6 317 modification besides Mg# equilibration and have erupted at the surface. This probably reflects the
7
8 318 tectonic setting of western Aleutian rhyodacite volcanoes (Yogodzinski et al., 2015), which lie only 40–50
9
10 319 km above the top of the slab and just east of a physical opening in the subducting plate (Levin et al.,
11
12 320 2005; Hayes et al., 2018). In this setting significant melt production is expected because the temperature
13
14 321 of the subducting oceanic crust must be well above the hydrous basalt solidus. The shallow depth means
15
16 322 that, in turn, any melt that escapes the slab will have a relatively short pathway to the surface, thus
17
18 323 limiting thermal and chemical exchange between the silicic melt and ambient mantle peridotite.

19 324 More commonly, however, ascending hydrous slab melts will trigger partial melting of the mantle
20
21 325 wedge when the wet peridotite solidus is exceeded (Kelemen, 1995; Pirard and Hermann, 2015). Mixing
22
23 326 with peridotite melts will attenuate the trace element and $\delta^{49/47}\text{Ti}$ slab melt signature and produce a wide
24
25 327 array of primary arc magma compositions that are blends of slab- and peridotite-derived melt.
26
27 328 Nevertheless, elevated $\delta^{49/47}\text{Ti}$ compared to N-MORB remains a uniquely sensitive tracer for the
28
29 329 involvement of a slab melt even when this is diluted with peridotite melt in transit through the mantle
30
31 330 wedge (Figure 4b).

32
33
34 331 Furthermore, the striking correlation between $\delta^{49/47}\text{Ti}$ and SiO_2 content of primitive arc lavas (Figure
35
36 332 5) suggests that the elevated silica content of primitive (Mg# ≥ 60) andesites and (rhyo)dacites found
37
38 333 worldwide (e.g., Kelemen et al., 2014) is a direct consequence of slab melting. We reiterate that although
39
40 334 fluid-fluxed melting of mantle wedge peridotite can produce andesitic melts with high Mg# (e.g., Kushiro,
41
42 335 1972; Till et al., 2012), the lack of Ti mobility in fluids means that such partial melts do not have the
43
44 336 elevated $\delta^{49/47}\text{Ti}$ found in primitive andesites and (rhyo)dacites (Figure 5). Hence, Ti isotope systematics
45
46 337 of primitive arc lavas provide strong support for slab melts as a key medium for mass transfer in
47
48 338 subduction zones.

49
50
51 339

52 340 **5.5. A recipe for widespread slab melting**

53
54
55 341 The specific sensitivity of Ti isotopes to slab melting allows us to identify at least one sample with a slab melt
56
57 342 component in all eight subduction zones for which $\delta^{49/47}\text{Ti}$ compositions of primitive arc lavas are available
58
59 343 (Figure 5). Primitive andesites and rhyodacites from the Aleutian arc, Cook Island, and Solander Islands have
60
61

1
2
3
4
5
6
7
8
9
10
11
12
13
14
15
16
17
18
19
20
21
22
23
24
25
26
27
28
29
30
31
32
33
34
35
36
37
38
39
40
41
42
43
44
45
46
47
48
49
50
51
52
53
54
55
56
57
58
59
60
61
62
63
64
65

344 previously been interpreted in the light of a significant slab melt contribution (e.g., Kay, 1978; Yogodzinski et
345 al., 1995; Stern and Kilian, 1996; Foley et al., 2014; Yogodzinski et al., 2017; see supplementary material),
346 which is confirmed by the new Ti isotope data, but also arcs where primitive silicic magmas are rare show
347 evidence for slab melting. For example, a reappraisal of previously published $\delta^{49/47}\text{Ti}$ data for the New Britain
348 arc and Mariana arc (Millet and Dauphas, 2014; Millet et al., 2016) leads us to recognize that one out of two
349 New Britain, and two out of three Mariana primitive lavas show a combination of elevated SiO_2 content and
350 $\delta^{49/47}\text{Ti}$ (ca. 0.05‰) relative to N-MORB (Figure 5) that could be indicative of a modest but clearly resolvable
351 slab melt contribution, though a more systematic study of Mariana and New Britain arc lavas is needed to
352 substantiate this. Moreover, primitive basaltic andesites from the Aegean arc show clear Ti isotope evidence
353 for an important role for slab melting ($\delta^{49/47}\text{Ti} = \text{ca. } 0.10\text{‰}$) whereas this had hitherto not been explicitly
354 demonstrated. In the Lesser Antilles arc, there is no unambiguous Ti isotope evidence for slab melting in the
355 southern islands (Grenada, St. Vincent, Bequia). The single sample from Saba, the northernmost active volcanic
356 centre of the Lesser Antilles arc, does display elevated $\delta^{49/47}\text{Ti}$ (0.06‰; Figure 4). The combined SiO_2 – $\delta^{49/47}\text{Ti}$
357 signature of this samples falls on the primitive arc lava array in Figure 5, consistent with a slab melt
358 contribution, but lavas from Saba show evidence for magma mixing (Defant et al., 2001) and this process
359 cannot be completely ruled out. In general, however, slab melting seems to be a widespread phenomenon in
360 modern subduction zones.

361 The prevalence of slab melting in modern subduction zones raises the question of which conditions are
362 required to allow melting of the subducted slab. Slab melting has often been related to the subduction of
363 young and warm oceanic crust (e.g., Defant and Drummond, 1990). Recent dynamic models (Syracuse et al.,
364 2010; van Keken et al., 2011; van Keken et al., 2018) and geochemical thermometry (Cooper et al., 2012),
365 however, suggest that the temperature required for slab melting can be met in the majority of modern
366 subduction zones. Based on the Ti isotope evidence for widespread slab melting, it appears that slab age is not
367 the defining parameter that dictates whether the slab can melt. For example, the Aegean arc has the oldest
368 (ca. 200 Ma) and therefore coldest subducting oceanic crust globally, yet lavas with a strong slab melt
369 signature are erupted. Rather than slab age, the three-dimensional structure of the slab likely plays a pivotal
370 role in providing additional sources of heat. In particular, tearing of the slab allows the inflow of
371 asthenospheric mantle that can heat the torn edge of the slab. This explanation has been invoked for the

372 melting of the 50–60 Ma Pacific slab in the western Aleutian arc (Yogodzinski et al., 2001; Levin et al.,
373 2005; Yogodzinski et al., 2017) and can also apply to the Aegean arc where lavas from Nisyros display Pb
374 isotope evidence for toroidal mantle flow through a slab tear (Klaver et al., 2016).

375 Another prerequisite for slab melting is the presence of aqueous fluids to lower the solidus of the
376 metabasite and metasediment. Insufficient water is probably present in the protolith at sub-arc depths to
377 allow dehydration melting (e.g., Spandler and Pirard, 2013), and hence an external fluid source is
378 required. Strontium isotope constraints suggest breakdown of serpentinite in the lithospheric mantle of
379 the slab as an important source of aqueous fluids (Yogodzinski et al., 2017; Klaver et al., 2020). These
380 fluids will travel up a temperature gradient in the slab and initiate hydrous partial melting when the wet
381 solidus of metabasite and/or metasediment is crossed. In cold subduction zones where the temperature
382 does not exceed the wet solidus of the slab, solute-rich aqueous fluids may still play an important role of
383 slab-to-mantle wedge mass transfer (e.g., Keppler, 2017; Rustioni et al., 2021) and contribute to island
384 arc basalt generation, but only slab melts can deliver fractionated Ti to the mantle wedge and produce
385 silicic primitive arc magmas.

386 387 **6. Conclusions**

388 A comprehensive study of the Ti isotope composition of primitive arc lavas ($Mg\# \geq 60$) from eight global
389 subduction zones indicates that primitive arc lavas display pronounced Ti isotope heterogeneity compared to
390 basalts erupted at oceanic spreading centres (MORB) and within-plate settings. Normal MORB has
391 homogeneous $\delta^{49/47}Ti$ ($0.001 \pm 0.015\%$), consistent with an absence of Ti isotope fractionation during
392 peridotite melting. In contrast, primitive arc lavas have strongly correlated $\delta^{49/47}Ti$ and SiO_2 contents with the
393 highest $\delta^{49/47}Ti$ ($0.24 \pm 0.03\%$) recorded in primitive rhyodacites from the western Aleutian arc. The
394 fractionated Ti isotope signature reflects melting in the presence of residual rutile, which can only plausibly
395 take place in the subducted oceanic crust and its sedimentary cover. Hence, $\delta^{49/47}Ti$ is a robust tracer of slab
396 melting even when slab melts are diluted during interaction with the mantle wedge. The conclusions from this
397 study can furthermore be summarised as follows:

- 398 • The modelled $\delta^{49/47}Ti$ of hydrous metabasite partial melts at 750–800 °C and 2.6–4.5 GPa
399 ($0.24 \pm 0.06\%$) matches that of primitive Aleutian rhyodacites ($0.24 \pm 0.03\%$), indicating that these

400 Aleutian rhyodacites are slab melts that have traversed the mantle wedge with only little modification
1
2 401 in the form of Mg# equilibration.

3
4 402 • The elevated $\delta^{49/47}\text{Ti}$ of primitive andesites and rhyodacites rules out their generation through
5
6 403 hydrous peridotite melting as the fractionated Ti signature cannot be carried to the mantle wedge by
7
8 404 aqueous fluids and rutile is not stable in peridotite melting residua.

9
10 405 • In addition to the Aleutian arc, all other studied subduction zones also display evidence for slab
11
12 406 melting, but in a more diluted form. Hydrous, silicic slab melts in transit through the mantle wedge
13
14 407 promote additional peridotite melting, which dilutes the original slab melt signature and generates a
15
16 408 wide spectrum of primary arc magmas that are blends of slab- and peridotite-derived melt.

17
18 409 • Slab melting therefore appears to be a common, widespread phenomenon in modern subduction
19
20 410 zones, irrespective of slab age. Rather, three-dimensional effects such as the presence of slab tears
21
22 411 can help raise the temperature of subducting slabs above their wet solidus. The influx of fluids
23
24 412 released by serpentinite breakdown will then trigger hydrous melting of the oceanic crust and
25
26 413 superjacent sediments.

27
28
29
30 414

31 32 415 **Acknowledgements**

33
34 416 This manuscript greatly benefitted from discussions with Pierre Bouilhol, Ben Maunder, Jeroen van Hunen, Tim
35
36 417 Elliott, Julie Prytulak, and Nikitha Saji. Jon Blundy and Richard Robertson are thanked for providing some of the
37
38 418 Lesser Antilles samples; Felix Genske and Heidi Beier are thanked for their assistance with Sr–Nd isotope
39
40 419 measurements made in Münster. Comments made by Steve Turner and an anonymous reviewer helped to
41
42 420 improve this work. Rosemary Hickey-Vargas is thanked for editorial handling. This work was supported by
43
44 421 NERC project NIIICE (NE/R001332/1) and a Royal Society Research Grant (RG150693) to MAM, as well as U.S.
45
46 422 National Science Foundation grants to GY (OCE-1551640, EAR-1753518).

47
48
49 423

50 51 424 **CRedit author statement**

52
53 425 **Martijn Klaver:** Conceptualization, Formal Analysis, Investigation, Writing – Original Draft; **Gene Yogodzinski:**
54
55 426 Conceptualization, Resources, Writing – Review & Editing, Funding Acquisition; **Capucine Albert:** Investigation;
56
57 427 **Michal Camejo-Harry:** Resources; **Marlina Elburg:** Resources; **Kaj Hoernle:** Resources; **Colin Macpherson:**
58
59 428 Resources, Writing – Review & Editing; **Geoff Nowell:** Resources; **Tracy Rushmer:** Resources, Writing – Review

1
2 429 & Editing; **Helen Williams**: Resources, Writing – Review & Editing; **Marc-Alban Millet**: Conceptualization,
3 Investigation, Writing – Review & Editing, Funding Acquisition.

4 431

5
6 432

7
8 433 **REFERENCES**

9
10 434

11
12 435 Aarons, S.M., Dauphas, N., Blanchard, M., Zeng, H., Nie, N.X., Johnson, A.C., Greber, N.D., Hopp, T., 2021. Clues
13 from ab initio calculations on titanium isotopic fractionation in tholeiitic and calc-alkaline magma
14 series. *ACS earth and space chemistry* 5, 2466-2480.
15 436

16
17 437
18 438 Alonso-Perez, R., Müntener, O., Ulmer, P., 2009. Igneous garnet and amphibole fractionation in the roots of
19 island arcs: experimental constraints on andesitic liquids. *Contrib. Mineral. Petrol.* 157, 541-558.
20 439

21 440 Carter, L.B., Skora, S., Blundy, J., De Hoog, J., Elliott, T., 2015. An experimental study of trace element fluxes
22 from subducted oceanic crust. *J. Petrol.* 56, 1585-1606.
23 441

24 442 Codillo, E., Le Roux, V., Marschall, H., 2018. Arc-like magmas generated by mélange-peridotite interaction in
25 the mantle wedge. *Nature communications* 9, 1-11.
26 443

27 444 Coldwell, B., Adam, J., Rushmer, T., Macpherson, C., 2011. Evolution of the East Philippine Arc: experimental
28 constraints on magmatic phase relations and adakitic melt formation. *Contrib. Mineral. Petrol.* 162,
29 835-848.
30 445

31 446
32 447 Cooper, L.B., Ruscitto, D.M., Plank, T., Wallace, P.J., Syracuse, E.M., Manning, C.E., 2012. Global variations in
33 H₂O/Ce: 1. Slab surface temperatures beneath volcanic arcs. *Geochem. Geophys. Geosyst.* 13.
34 448

35 449 Defant, M.J., Drummond, M.S., 1990. Derivation of some modern arc magmas by melting of young subducted
36 lithosphere. *Nature* 347, 662-665.
37 450

38 451 Defant, M.J., Sherman, S., Maury, R.C., Bellon, H., De Boer, J., Davidson, J., Kepezhinskas, P., 2001. The geology,
39 petrology, and petrogenesis of Saba Island, Lesser Antilles. *J. Volcanol. Geotherm. Res.* 107, 87-111.
40 452

41 453 Deng, Z., Moynier, F., Sossi, P., Chaussidon, M., 2018. Bridging the depleted MORB mantle and the continental
42 crust using titanium isotopes. *Geochemical Perspectives Letters* 9, 11-15.
43 454

44 455 Deng, Z., Chaussidon, M., Savage, P., Robert, F., Pik, R., Moynier, F., 2019. Titanium isotopes as a tracer for the
45 plume or island arc affinity of felsic rocks. *Proceedings of the National Academy of Sciences* 116,
46 1132-1135.
47 457

- 1
2 458 Deng, Z., Schiller, M., Jackson, M.G., Millet, M.-A., Pan, L., Nikolajsen, K., Saji, N.S., Huang, D., Bizzarro, M.,
3 459 2023. Earth's evolving geodynamic regime recorded by titanium isotopes. *Nature* 621, 100-104.
4 460 Elburg, M.A., Smet, I., De Pelsmaeker, E., 2014. Influence of source materials and fractionating assemblage on
5 461 magmatism along the Aegean Arc, and implications for crustal growth. Geological Society, London,
6 462 Special Publications 385, 137-160.
7
8 463 Elliott, T., Plank, T., Zindler, A., White, W., Bourdon, B., 1997. Element transport from slab to volcanic front at
9 464 the Mariana arc. *Journal of Geophysical Research: Solid Earth* 102, 14991-15019.
10
11 465 Foley, F.V., Turner, S., Rushmer, T., Caulfield, J.T., Daczko, N.R., Bierman, P., Robertson, M., Barrie, C.D., Boyce,
12 466 A.J., 2014. ^{10}Be , ^{18}O and radiogenic isotopic constraints on the origin of adakitic signatures: a case
13 467 study from Solander and Little Solander Islands, New Zealand. *Contrib. Mineral. Petrol.* 168, 1-28.
14
15 468 Gaetani, G.A., Asimow, P.D., Stolper, E.M., 2008. A model for rutile saturation in silicate melts with
16 469 applications to eclogite partial melting in subduction zones and mantle plumes. *Earth Planet. Sci. Lett.*
17 470 272, 720-729.
18
19 471 Gill, J., 1981. *Orogenic andesites and plate tectonics*. Springer, Berlin.
20
21 472 Greber, N.D., Dauphas, N., Bekker, A., Ptáček, M.P., Bindeman, I.N., Hofmann, A., 2017. Titanium isotopic
22 473 evidence for felsic crust and plate tectonics 3.5 billion years ago. *Science* 357, 1271-1274.
23
24 474 Greber, N.D., Pettke, T., Vilela, N., Lanari, P., Dauphas, N., 2021. Titanium isotopic compositions of bulk rocks
25 475 and mineral separates from the Kos magmatic suite: Insights into fractional crystallization and magma
26 476 mixing processes. *Chem. Geol.* 578, 120303.
27
28 477 Grove, T.L., Chatterjee, N., Parman, S.W., Médard, E., 2006. The influence of H_2O on mantle wedge melting.
29 478 *Earth Planet. Sci. Lett.* 249, 74-89.
30
31 479 Hayes, G.P., Moore, G.L., Portner, D.E., Hearne, M., Flamme, H., Furtney, M., Smoczyk, G.M., 2018. Slab2, a
32 480 comprehensive subduction zone geometry model. *Science* 362, 58-61.
33
34 481 Hermann, J., Spandler, C., Hack, A., Korsakov, A.V., 2006. Aqueous fluids and hydrous melts in high-pressure
35 482 and ultra-high pressure rocks: Implications for element transfer in subduction zones. *Lithos* 92, 399-
36 483 417.
37
38 484 Hernández-Urbe, D., Hernández-Montenegro, J.D., Cone, K.A., Palin, R.M., 2020. Oceanic slab-top melting
39 485 during subduction: Implications for trace-element recycling and adakite petrogenesis. *Geology* 48,
40 486 216-220.
41
42
43
44
45
46
47
48
49
50
51
52
53
54
55
56
57
58
59
60
61
62
63
64
65

- 1
2
3
4
5
6
7
8
9
10
11
12
13
14
15
16
17
18
19
20
21
22
23
24
25
26
27
28
29
30
31
32
33
34
35
36
37
38
39
40
41
42
43
44
45
46
47
48
49
50
51
52
53
54
55
56
57
58
59
60
61
62
63
64
65
- 487 Hoare, L., Klaver, M., Saji, N.S., Gillies, J., Parkinson, I.J., Lissenberg, C.J., Millet, M.-A., 2020. Melt chemistry
488 and redox conditions control titanium isotope fractionation during magmatic differentiation.
489 *Geochim. Cosmochim. Acta* 282, 38-54.
- 490 Hoare, L., Klaver, M., Muir, D.D., Klemme, S., Barling, J., Parkinson, I.J., Lissenberg, C.J., Millet, M.-A., 2022.
491 Empirical and experimental constraints on Fe-Ti oxide-melt titanium isotope fractionation factors.
492 *Geochim. Cosmochim. Acta* 326, 253-272.
- 493 Johnson, M.C., Plank, T., 1999. Dehydration and melting experiments constrain the fate of subducted
494 sediments. *Geochem. Geophys. Geosyst.* 1.
- 495 Kay, R.W., 1978. Aleutian magnesian andesites: melts from subducted Pacific Ocean crust. *J. Volcanol.*
496 *Geotherm. Res.* 4, 117-132.
- 497 Kelemen, P.B., 1995. Genesis of high Mg# andesites and the continental crust. *Contrib. Mineral. Petrol.* 120, 1-
498 19.
- 499 Kelemen, P.B., Hanghøj, K., Greene, A.R., 2014. One view of the geochemistry of subduction-related magmatic
500 arcs, with an emphasis on primitive andesite and lower crust, in: Holland, H.D., Turekian, K.K. (Eds.),
501 *Treatise on geochemistry* (2nd edition). Elsevier, Oxford, pp. 749-805.
- 502 Keppler, H., 2017. Fluids and trace element transport in subduction zones. *Am. Mineral.* 102, 5-20.
- 503 Kessel, R., Schmidt, M.W., Ulmer, P., Pettke, T., 2005a. Trace element signature of subduction-zone fluids,
504 melts and supercritical liquids at 120–180 km depth. *Nature* 437, 724-727.
- 505 Kessel, R., Ulmer, P., Pettke, T., Schmidt, M., Thompson, A., 2005b. The water–basalt system at 4 to 6 GPa:
506 Phase relations and second critical endpoint in a K-free eclogite at 700 to 1400 C. *Earth Planet. Sci.*
507 *Lett.* 237, 873-892.
- 508 Klaver, M., Davies, G.R., Vroon, P.Z., 2016. Subslab mantle of African provenance infiltrating the Aegean
509 mantle wedge. *Geology* 44, 367-370.
- 510 Klaver, M., Lewis, J., Parkinson, I.J., Elburg, M.A., Vroon, P.Z., Kelley, K.A., Elliott, T., 2020. Sr isotopes in arcs
511 revisited: tracking slab dehydration using $\delta^{88/86}\text{Sr}$ and $^{87}\text{Sr}/^{86}\text{Sr}$ systematics of arc lavas. *Geochim.*
512 *Cosmochim. Acta* 288, 101-119.
- 513 Klaver, M., MacLennan, S.A., Ibañez-Mejía, M., Tissot, F.L.H., Vroon, P.Z., Millet, M.-A., 2021. Reliability of
514 detrital marine sediments as proxy for continental crust composition: The effects of hydrodynamic
515 sorting on Ti and Zr isotope systematics. *Geochim. Cosmochim. Acta* 310, 221-239.

- 516 Kommescher, S., Kurzweil, F., Fonseca, R.O.C., Rzehak, L.J.A., Hohl, S.V., Kirchenbaur, M., Schuth, S., Sprung, P.,
1
2 517 Munker, C., 2023. Mineralogical Controls on the Ti Isotope Composition of Subduction Zone Magmas.
3
4 518 Geochem. Geophys. Geosyst. 24, e2022GC010840.
5
6 519 Kushiro, I., 1972. Effect of water on the composition of magmas formed at high pressures. J. Petrol. 13, 311-
7
8 520 334.
9
10 521 Lara, M., Dasgupta, R., 2020. Partial melting of a depleted peridotite metasomatized by a MORB-derived
11
12 522 hydrous silicate melt—Implications for subduction zone magmatism. Geochim. Cosmochim. Acta 290,
13
14 523 137-161.
15
16
17 524 Levin, V., Shapiro, N.M., Park, J., Ritzwoller, M.H., 2005. Slab portal beneath the western Aleutians. Geology
18
19 525 33, 253-256.
20
21 526 Li, H., Hermann, J., Zhang, L., 2022. Melting of subducted slab dictates trace element recycling in global arcs.
22
23 527 Science Advances 8, eabh2166.
24
25 528 Macpherson, C.G., Dreher, S.T., Thirlwall, M.F., 2006. Adakites without slab melting: high pressure
26
27 529 differentiation of island arc magma, Mindanao, the Philippines. Earth Planet. Sci. Lett. 243, 581-593.
28
29
30 530 Mann, U., Schmidt, M.W., 2015. Melting of pelitic sediments at subarc depths: 1. Flux vs. fluid-absent melting
31
32 531 and a parameterization of melt productivity. Chem. Geol. 404, 150-167.
33
34 532 Martin, L.A., Hermann, J., 2018. Experimental phase relations in altered oceanic crust: implications for carbon
35
36 533 recycling at subduction zones. J. Petrol. 59, 299-320.
37
38 534 Martindale, M., Skora, S., Pickles, J., Elliott, T., Blundy, J., Avanzinelli, R., 2013. High pressure phase relations of
39
40 535 subducted volcanoclastic sediments from the west pacific and their implications for the geochemistry
41
42 536 of Mariana arc magmas. Chem. Geol. 342, 94-109.
43
44
45 537 Millet, M.-A., Dauphas, N., 2014. Ultra-precise titanium stable isotope measurements by double-spike high
46
47 538 resolution MC-ICP-MS. J. Anal. At. Spectrom. 29, 1444-1458.
48
49 539 Millet, M.-A., Dauphas, N., Greber, N.D., Burton, K.W., Dale, C.W., Debret, B., Macpherson, C.G., Nowell, G.M.,
50
51 540 Williams, H.M., 2016. Titanium stable isotope investigation of magmatic processes on the Earth and
52
53 541 Moon. Earth Planet. Sci. Lett. 449, 197-205.
54
55
56 542 Nielsen, S.G., Marschall, H.R., 2017. Geochemical evidence for mélangé melting in global arcs. Science
57
58 543 Advances 3, e1602402.
59
60
61
62
63
64
65

- 544 Pirard, C., Hermann, J., 2015. Focused fluid transfer through the mantle above subduction zones. *Geology* 43,
1
2 545 915-918.
3
- 4 546 Plank, T., Langmuir, C.H., 1993. Tracing trace elements from sediment input to volcanic output at subduction
5
6 547 zones. *Nature* 362, 739-743.
7
- 8 548 Plank, T., Langmuir, C.H., 1998. The chemical composition of subducting sediment and its consequences for the
9
10 549 crust and mantle. *Chem. Geol.* 145, 325-394.
11
- 12 550 Rapp, R., Shimizu, N., Norman, M., Applegate, G., 1999. Reaction between slab-derived melts and peridotite in
13
14 551 the mantle wedge: experimental constraints at 3.8 GPa. *Chem. Geol.* 160, 335-356.
15
- 16 552 Rebaza, A.M., Mallik, A., Straub, S.M., 2023. Multiple episodes of rock-melt reaction at the slab-mantle
17
18 553 interface: Formation of high silica primary magmas in intermediate to hot subduction zones. *J. Petrol.*
19
20 554 64, 1-20.
21
- 22 555 Rustioni, G., Audetat, A., Keppler, H., 2021. The composition of subduction zone fluids and the origin of the
23
24 556 trace element enrichment in arc magmas. *Contrib. Mineral. Petrol.* 176, 51.
25
- 26 557 Ryerson, F.J., Watson, E.B., 1987. Rutile saturation in magmas: implications for Ti-Nb-Ta depletion in island-arc
27
28 558 basalts. *Earth Planet. Sci. Lett.* 86, 225-239.
29
- 30 559 Rzehak, L.J., Kommescher, S., Kurzweil, F., Sprung, P., Leitzke, F.P., Fonseca, R.O., 2021. The redox dependence
31
32 560 of titanium isotope fractionation in synthetic Ti-rich lunar melts. *Contrib. Mineral. Petrol.* 176, 1-16.
33
- 34 561 Rzehak, L.J.A., Kommescher, S., Hoare, L., Kurzweil, F., Sprung, P., Leitzke, F.P., Fonseca, R.O.C., 2022. Redox-
35
36 562 dependent Ti stable isotope fractionation on the Moon: implications for current lunar magma ocean
37
38 563 models. *Contrib. Mineral. Petrol.* 177, 1-20.
39
- 40 564 Schmidt, M.W., Vielzeuf, D., Auzanneau, E., 2004. Melting and dissolution of subducting crust at high
41
42 565 pressures: the key role of white mica. *Earth Planet. Sci. Lett.* 228, 65-84.
43
- 44 566 Sisson, T., Kelemen, P., 2018. Near-solidus melts of MORB + 4 wt% H₂O at 0.8–2.8 GPa applied to issues of
45
46 567 subduction magmatism and continent formation. *Contrib. Mineral. Petrol.* 173, 1-23.
47
- 48 568 Skora, S., Blundy, J., 2010. High-pressure hydrous phase relations of radiolarian clay and implications for the
49
50 569 involvement of subducted sediment in arc magmatism. *J. Petrol.* 51, 2211-2243.
51
- 52 570 Skora, S., Blundy, J.D., Brooker, R.A., Green, E.C., de Hoog, J., Connolly, J.A., 2015. Hydrous phase relations and
53
54 571 trace element partitioning behaviour in calcareous sediments at subduction-zone conditions. *J. Petrol.*
55
56 572 56, 953-980.
57
58
59
60
61
62
63
64
65

- 573 Spandler, C., Pirard, C., 2013. Element recycling from subducting slabs to arc crust: a review. *Lithos* 170, 208-
1 223.
2
3
4 575 Stern, C.R., Kilian, R., 1996. Role of the subducted slab, mantle wedge and continental crust in the generation
5
6 576 of adakites from the Andean Austral Volcanic Zone. *Contrib. Mineral. Petrol.* 123, 263-281.
7
8 577 Syracuse, E.M., van Keken, P.E., Abers, G.A., 2010. The global range of subduction zone thermal models. *Phys.*
9
10 578 *Earth Planet. Inter.* 183, 73-90.
11
12 579 Tatsumi, Y., 1989. Migration of fluid phases and genesis of basalt magmas in subduction zones. *Journal of*
13
14 580 *Geophysical Research: Solid Earth* 94, 4697-4707.
15
16 581 Tera, F., Brown, L., Morris, J., Sacks, I.S., Klein, J., Middleton, R., 1986. Sediment incorporation in island-arc
17
18 582 magmas: Inferences from ¹⁰Be. *Geochim. Cosmochim. Acta* 50, 535-550.
19
20 583 Till, C.B., Grove, T.L., Withers, A.C., 2012. The beginnings of hydrous mantle wedge melting. *Contrib. Mineral.*
21
22 584 *Petrol.* 163, 669-688.
23
24 585 Turner, S.J., Langmuir, C.H., 2022a. A quantitative framework for global variations in arc geochemistry. *Earth*
25
26 586 *Planet. Sci. Lett.* 584, 117411.
27
28 587 Turner, S.J., Langmuir, C.H., 2022b. Sediment and ocean crust both melt at subduction zones. *Earth Planet. Sci.*
29
30 588 *Lett.* 584, 117424.
31
32 589 van Keken, P.E., Hacker, B.R., Syracuse, E.M., Abers, G.A., 2011. Subduction factory: 4. Depth-dependent flux of
33
34 590 H₂O from subducting slabs worldwide. *Journal of Geophysical Research: Solid Earth* 116.
35
36 591 van Keken, P.E., Wada, I., Abers, G.A., Hacker, B.R., Wang, K., 2018. Mafic high-pressure rocks are
37
38 592 preferentially exhumed from warm subduction settings. *Geochem. Geophys. Geosyst.* 19, 2934-2961.
39
40 593 White, W.M., Dupré, B., 1986. Sediment subduction and magma genesis in the Lesser Antilles: isotopic and
41
42 594 trace element constraints. *Journal of Geophysical Research: Solid Earth (1978–2012)* 91, 5927-5941.
43
44 595 Xiong, X., Keppler, H., Audétat, A., Gudfinnsson, G., Sun, W., Song, M., Xiao, W., Yuan, L., 2009. Experimental
45
46 596 constraints on rutile saturation during partial melting of metabasalt at the amphibolite to eclogite
47
48 597 transition, with applications to TTG genesis. *Am. Mineral.* 94, 1175-1186.
49
50 598 Yogodzinski, G., Kay, R., Volynets, O., Koloskov, A., Kay, S., 1995. Magnesian andesite in the western Aleutian
51
52 599 Komandorsky region: implications for slab melting and processes in the mantle wedge. *Geol. Soc. Am.*
53
54 600 *Bull.* 107, 505-519.
55
56
57
58
59
60
61
62
63
64
65

601 Yogodzinski, G., Lees, J., Churikova, T., Dorendorf, F., Wöerner, G., Volynets, O., 2001. Geochemical evidence
602 for the melting of subducting oceanic lithosphere at plate edges. *Nature* 409, 500-504.
603 Yogodzinski, G.M., Brown, S.T., Kelemen, P.B., Vervoort, J.D., Portnyagin, M., Sims, K.W., Hoernle, K., Jicha,
604 B.R., Werner, R., 2015. The role of subducted basalt in the source of island arc magmas: evidence
605 from seafloor lavas of the western Aleutians. *J. Petrol.* 56, 441-492.
606 Yogodzinski, G.M., Kelemen, P.B., Hoernle, K., Brown, S.T., Bindeman, I., Vervoort, J.D., Sims, K.W., Portnyagin,
607 M., Werner, R., 2017. Sr and O isotopes in western Aleutian seafloor lavas: Implications for the source
608 of fluids and trace element character of arc volcanic rocks. *Earth Planet. Sci. Lett.* 475, 169-180.

609
610

611 FIGURE CAPTIONS

612

613 **Figure 1.** Kernel density diagram for primitive arc lavas ($Mg\# \geq 60$) compared to normal mid ocean ridge basalts
614 (N-MORB; Millet et al., 2016; Deng et al., 2018) and ocean island basalts (OIB) plus enriched MORB (Millet et
615 al., 2016; Deng et al., 2018; Deng et al., 2019; Hoare et al., 2020; Deng et al., 2023). See supplementary
616 Dataset 2 for all data. The field for the bulk silicate Earth (BSE) is from Millet et al. (2016). Primitive arc lavas
617 have $\delta^{49/47}Ti$ that extends to higher values than MORB.

618

619 **Figure 2.** The modelled magnitude of Ti isotope fractionation during hydrous melting of (altered) MORB (A)
620 and various sediment lithologies (B) at 2.6–6 GPa, expressed as $\Delta^{49/47}Ti_{melt-protolith}$, which is the difference in
621 $\delta^{49/47}Ti$ between the partial melt and the protolith. Experimental studies (Schmidt et al., 2004; Kessel et al.,
622 2005b; Skora and Blundy, 2010; Martindale et al., 2013; Carter et al., 2015; Mann and Schmidt, 2015; Skora et
623 al., 2015; Martin and Hermann, 2018; Sisson and Kelemen, 2018) yield the phase proportions and Ti content of
624 the partial melt and residual minerals after which $\Delta^{49/47}Ti_{melt-protolith}$ is calculated by isotopic mass balance using
625 Ti isotope mineral–melt fractionation factors (supplementary Tables S1 and 2). Rutile is invariably present as a
626 residual phase during hydrous melting of metabasite and metasediment, which imposes an isotopically heavy
627 Ti isotope signature on the partial melt. Some symbols are shifted slightly to higher or lower temperature (≤ 5
628 °C unless indicated) to prevent cluttering of the datapoints. The open symbols in panel B denote experiments
629 where both titanomagnetite (≥ 0.5 wt.% abundance) and rutile are present as residual phase. The grey field

630 shows the Ti isotope fractionation of 2–25% anhydrous partial melts of a fertile peridotite at 1–2.5 GPa. See
631 supplementary material for a detailed description of the modelling approach and parameters used; the
632 melting models are provided in supplementary Dataset 1. A corresponding figure for the fractionation of the
633 melting residua relative to the protolith ($\Delta^{49/47}\text{Ti}_{\text{residue-protolith}}$) is provided in the supplementary material (Figure
634 S2).

635

636 **Figure 3.** Effects of magmatic differentiation on the Ti isotope composition of arc lavas. (A) Fractional
637 crystallization of isotopically light titanomagnetite (Ti-mag) drives arc lavas to high $\delta^{49/47}\text{Ti}$. Two arc
638 differentiation suites are shown: a tholeiitic Kermadec and New Britain arcs trend, and a calc-alkaline trend
639 displayed by Santorini lavas (Aegean arc). Both suites show a clear inflection in $\delta^{49/47}\text{Ti}$ upon saturation of the
640 melt with titanomagnetite at Mg# 30–40. At higher Mg#, fractional crystallization of silicate minerals has
641 negligible effect on $\delta^{49/47}\text{Ti}$ and hence primitive arc lavas (PAL; Mg# ≥ 60) retain a primary Ti isotope signature.
642 (B) Titanium isotope effects of magma mixing. Two sets of mixing lines are shown between primitive lavas (St.
643 Vincent picrite RSV52, New Britain basalt 116852-5) and either evolved andesite (AAS-036), dacite (AAS-041),
644 or rhyodacite (AAS-033) from Santorini (Aegean arc). The mixing lines are dashed where Mg# < 60 . Magma
645 mixing cannot account for the $\delta^{49/47}\text{Ti}$ variation seen in global primitive arc lavas.

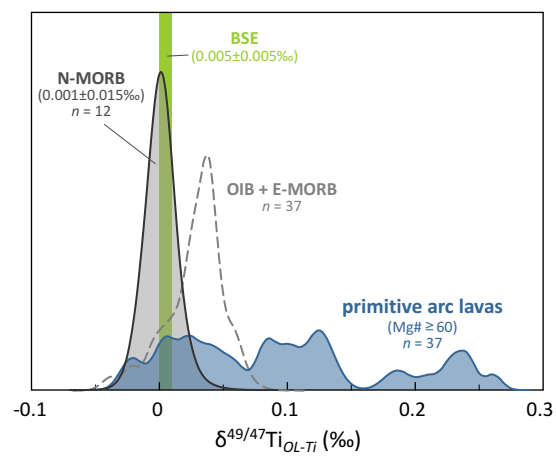
646

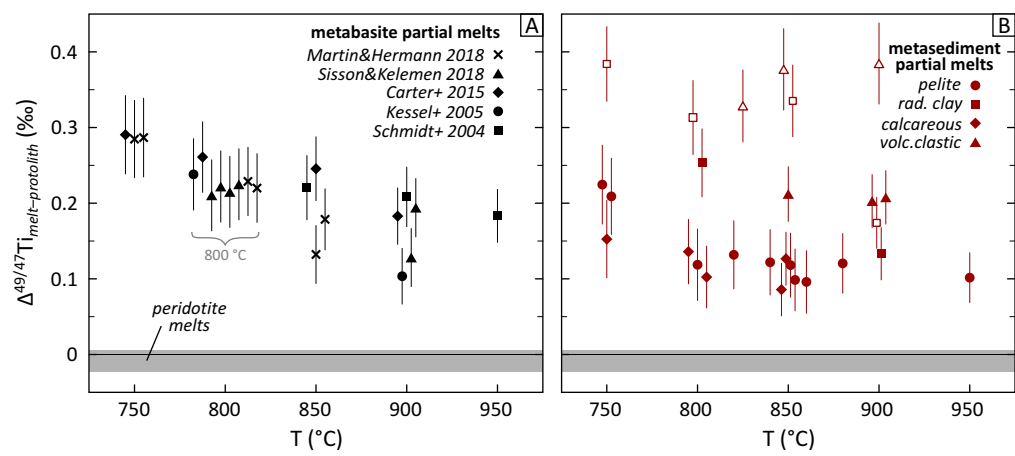
647 **Figure 4.** Variation in $\delta^{49/47}\text{Ti}$ of primitive arc lavas (Mg# ≥ 60) versus $^{143}\text{Nd}/^{144}\text{Nd}$; see supplementary Dataset 2
648 for all data shown in the figure. (A) Model curves showing binary mixing between a depleted mantle (DM)
649 source (0.05 wt.% TiO_2 , 0.4 $\mu\text{g/g}$ Nd) and bulk sediment subducting in the Aegean arc (Klaver et al., 2021) or
650 global subducting sediment (GLOSS; Plank and Langmuir, 1998) with $\delta^{49/47}\text{Ti}$ estimated at 0.24‰ (i.e., the
651 maximum of modern marine sediments; Greber et al., 2017). The compositions of N-MORB and OIB+E-MORB
652 are shown for comparison – see Figure 1 for data sources. (B) Model curves for mixing between a depleted
653 mantle (DM) source and hydrous partial melts of metabasite and metasediment. The composition of the
654 metabasite partial melt ($\delta^{49/47}\text{Ti} = 0.24\text{‰}$, 0.24 wt.% TiO_2) is the average $\Delta^{49/47}\text{Ti}_{\text{melt-protolith}}$ for metabasite at
655 750–800 °C (0.244‰; see Figure 2a) added to the average $\delta^{49/47}\text{Ti}$ of N-MORB (0.001‰; see Figure 1). The
656 metasediment partial melt ($\delta^{49/47}\text{Ti} = 0.34\text{‰}$, 0.17 wt.% TiO_2) is the average $\Delta^{49/47}\text{Ti}_{\text{melt-protolith}}$ for metasediment
657 (without titanomagnetite) at 750–800 °C (0.171‰; see Figure 2b) added to the average $\delta^{49/47}\text{Ti}$ of sediment
658 subducting in the Aegean arc (0.172‰; Klaver et al., 2021). Both metabasite and metasediment partial melt

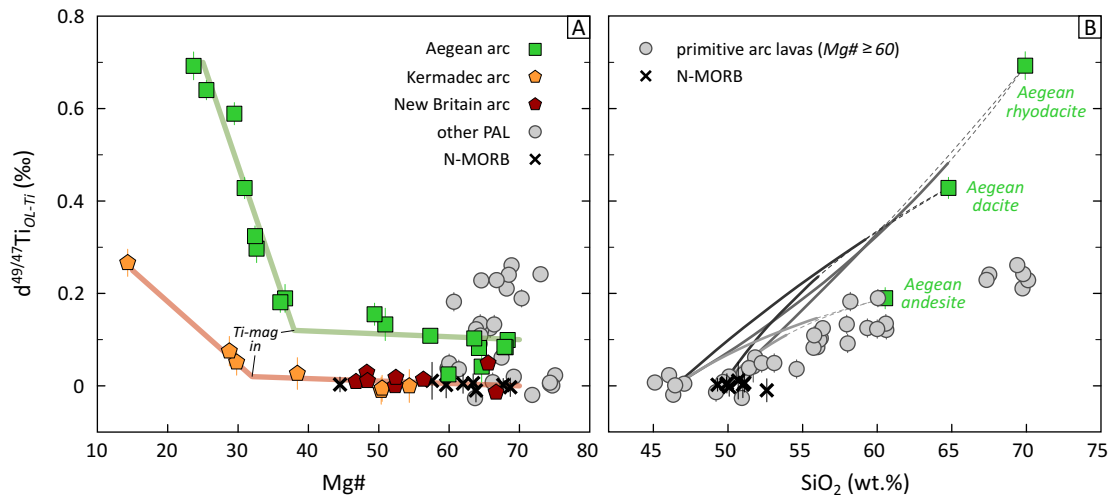
659 are assumed to have Ti/Nd of 55 (Martindale et al., 2013; Skora et al., 2015; Sisson and Kelemen, 2018).
1
2 660 Aleutian arc rhyodacites for which no Nd isotope data are available are plotted at the average $^{143}\text{Nd}/^{144}\text{Nd}$ of
3
4 661 similar samples from the Western Cones area where $^{143}\text{Nd}/^{144}\text{Nd}$ is homogeneous at 0.51312 ± 0.00004 . Sample
5
6 662 location abbreviations: Aeg – Aegean arc; Ale – Aleutian arc; LAn – Lesser Antilles arc; Mar – Mariana arc; NBr
7
8 663 – New Britain arc; Phi – Philippines arc; CI – Cook Island (Austral Volcanic Zone, Chile); SI – Solander Islands
9
10 664 (New Zealand).

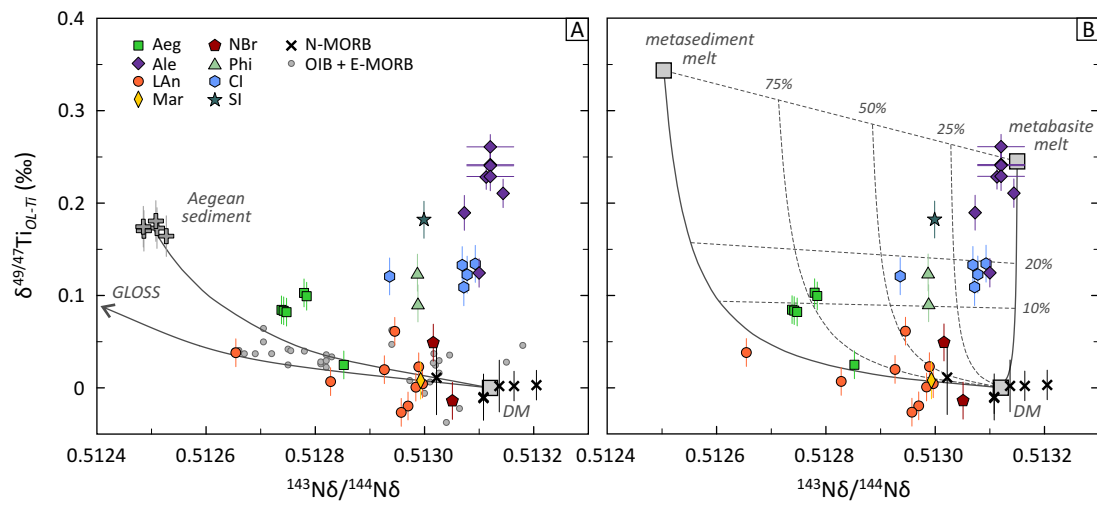
11
12 665

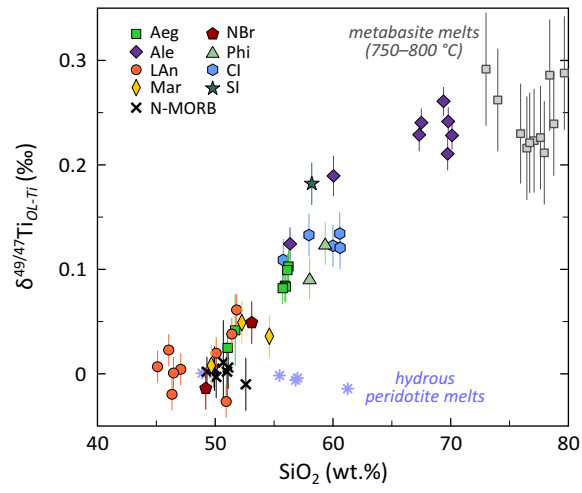
13
14
15 666 **Figure 5.** Primitive arc lavas ($\text{Mg\#} \geq 60$) display a strong correlation between $\delta^{49/47}\text{Ti}$ and SiO_2 content. The
16
17 667 composition of the metabasite partial melts at 750–800 °C (grey squares) is their $\Delta^{49/47}\text{Ti}_{\text{melt-protolith}}$ (Figure 2a)
18
19 668 added to the average $\delta^{49/47}\text{Ti}$ of N-MORB (0.001‰; see Figure 1). The composition of hydrous peridotite melts
20
21 669 is from experimental studies for peridotite+H₂O (Grove et al., 2006; Till et al., 2012) where $\delta^{49/47}\text{Ti}$ is calculated
22
23 670 though an isotopic mass balance (as in Figure 2; see supplementary material for details), assuming that no Ti is
24
25 671 transported to the mantle wedge by aqueous fluids (Rustioni et al., 2021) and mantle peridotite has $\delta^{49/47}\text{Ti} =$
26
27 672 0. Sample location abbreviations: Aeg – Aegean arc; Ale – Aleutian arc; LAn – Lesser Antilles arc; Mar –
28
29 673 Mariana arc; NBr – New Britain arc; Phi – Philippines arc; CI – Cook Island (Austral Volcanic Zone, Chile); SI –
30
31 674 Solander Islands (New Zealand).













Click here to access/download

Supplementary material for online publication only

Klaver Ti arc lavas supplementary
material_REVISED.pdf



[Click here to access/download](#)

Supplementary material for online publication only
Supplementary Dataset 1_melting models.xlsx





[Click here to access/download](#)

Supplementary material for online publication only
Supplementary Dataset 2_Ti isotope data.xlsx



Declaration of interests

The authors declare that they have no known competing financial interests or personal relationships that could have appeared to influence the work reported in this paper.

The authors declare the following financial interests/personal relationships which may be considered as potential competing interests: